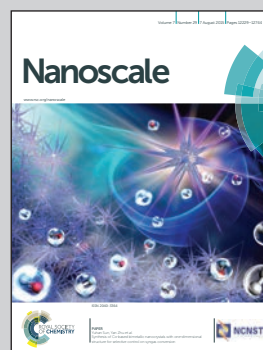**Showcasing research from Catalysis Research Center, Hokkaido University, Sapporo, Japan.**

Morphology-dependent photocatalytic activity of octahedral anatase particles prepared by ultrasonication–hydrothermal reaction of titanates

Direct correlation between morphology and photocatalytic activity has been found for octahedral-shaped anatase titania particles (OAPs). It is proposed that shallow electron traps are preferentially distributed on exposed {101} crystal facets of OAPs and govern the reactivity and the lifetime of photoexcited electrons, while deep electron traps (on which recombination of charge carriers occurs) are mainly formed in non-perfectly shaped particles.

ROYAL SOCIETY
OF **CHEMISTRY**

www.rsc.org/nanoscale

Nanoscale

Morphology-dependent photocatalytic activity of octahedral anatase particles prepared by ultrasonication–hydrothermal reaction of titanates†

Zhishun Wei,[a] Ewa Kowalska,*[a] Jonathan Verrett,[b] Christophe Colbeau-Justin,[b] Hynd Remita[b,c] and Bunsho Ohtani[a]

Octahedral anatase particles (OAPs) were prepared by an ultrasonication (US)–hydrothermal (HT) reaction of partially proton-exchanged potassium titanate nanowires (TNWs). The structural/physical properties of OAP-containing samples, including specific surface area, crystallinity, crystallite size, particle aspect ratio, composition and total OAP content, were analyzed. Photocatalytic activities of samples were measured under irradiation (>290 nm) for oxidative decomposition of acetic acid (CO_2 system) and dehydrogenation of methanol (H_2 system) under aerobic and deaerated conditions, respectively. Total density of electron traps (ETs) was measured by double-beam photoacoustic spectroscopy (DB-PAS). Mobility and lifetime of charge carriers (electrons) were investigated by the time-resolved microwave conductivity (TRMC) method. The effects of synthesis parameters, *i.e.*, HT duration, HT temperature and US duration, on properties and photocatalytic activities of final products were examined in detail. The sample prepared with 1 h US duration and 6 h HT duration at 433 K using 267 mg of TNWs in 80 mL of Milli-Q water exhibited the highest photocatalytic activity. It was found that change in HT duration or HT temperature while keeping the other conditions the same resulted in changes in all properties and photocatalytic activity. On the other hand, duration of US treatment, before HT reaction, influenced the morphology of both the reagent (by TNWs breaking) and final products (change in total OAP content); samples prepared with various US durations exhibited almost the same structural/physical properties evaluated in this study but were different in morphology and photocatalytic activity. This enabled clarification of the correlation between morphology and photocatalytic activity, *i.e.*, the higher the total OAP content was, the higher was the level of photocatalytic activity, especially in the CO_2 system. Although the decay after maximum TRMC signal intensity (I_{max}) was almost constant for all samples used in this study, photocatalytic activities were roughly proportional to I_{max}, which tended to be proportional to total OAP content. Assuming that I_{max} corresponds to the product of density of electrons in mobile shallow ETs and their mobility, the results suggest that OAP particles have beneficial shallow ETs in higher density and thereby the OAP content governs the photocatalytic activities. Thus, morphology-dependent photocatalytic activity of OAP-containing particles was reasonably interpreted by density of ETs presumably located on the exposed {101} facets.

[a]*Catalysis Research Center, Hokkaido University, Sapporo 001-0021, Japan.*
E-mail: kowalska@cat.hokudai.ac.jp; Fax: +81-11-706-9133; Tel: +81-11-706-9130
[b]*Laboratory of Physical Chemistry, UMR 8000, Paris-Sud University, 91405 Orsay, France*
[c]*CNRS, Laboratory of Physical Chemistry, UMR 8000, 91405 Orsay, France*
†Electronic supplementary information (ESI) available. See DOI: 10.1039/c5nr02386f

1 Introduction

Titanium(IV) oxide (titania) has been widely used for many years as a photocatalyst, presumably due to its advantages including high redox ability, stability and nontoxicity.[1–3] Another hidden reason for the popular use of titania as a photocatalyst is that titania shows appreciable (detectable) photocatalytic activity when purchased from any supplier or prepared through any procedure. Although fundamental mechanisms and widespread applications of titania photocatalysis, *e.g.*, for environmental purification and solar energy

conversion,[4,5] have been studied for at least 40 years, there are still many issues which should be explained and clarified.[6,7] The key property of high photocatalytic activity is one of those non-clarified issues, but there seems to be no effective way to clarify this issue since it is almost impossible to obtain a series of photocatalyst samples with a difference in only one structural/physical property and with no change in the other properties. A large number of papers showing correlations between structural/physical properties and photocatalytic activities have been published.[8–10] For example, it has been suggested that larger specific surface area, smaller crystalline size and higher crystallinity lead to higher photocatalytic activity.[11–13] However, as stated above, a direct correlation between one structural/physical property and photocatalytic activity cannot be proved since all structural properties change simultaneously when conditions of photocatalyst preparation and/or treatment are changed. As a result, the balance between different properties has often been suggested as a reason for the high level of photocatalytic activity.

Morphology-dependent or exposed facet-dependent activity of photocatalysts,[14] which has been widely studied for reactions occurring on titania single crystal (mainly rutile {110}),[15] has recently been investigated also for particulate photocatalysts using facetted polyhedral particles. To study the morphology-dependent photocatalytic activity of titania photocatalysts, octahedral anatase particles (OAPs) seem to be appropriate since they expose eight equivalent most thermodynamically stable {101} facets, the same as natural minerals of anatase titania.[16] We have recently developed an ultrasonication (US)–hydrothermal (HT) reaction to prepare OAPs, which exhibited high levels of photocatalytic activity for oxidation of acetic acid in comparison with the photocatalytic activities of many commercial titania samples with similar properties.[16,17]

An HT process has been widely used for the preparation of various materials with controlled morphology.[18–21] Conditions for the HT process, including HT duration, HT temperature, and pre-treatment and post-treatment operations, may influence the physical properties, morphology and photocatalytic activities of the resulting products. Generally speaking, a higher temperature and longer duration of the HT process result in increases in crystallinity[22] and crystalline size.[23–25] Thus, similar products may be obtained either by prolonging the HT duration[26] or increasing the HT temperature.[26] Prolonged HT duration, as well as post-treatment operations, can change the morphology of a product due to particle sintering.[25]

Although many papers showing the influence of morphology on photocatalytic activities have already been published,[27,28] there has been no report, except for our recent letter on OAPs,[29] showing a direct correlation between morphology and photocatalytic activity. We have found that OAP-containing products obtained with various durations of US prior to HT treatment showed variations in morphology and photocatalytic activity with all of the other properties remaining almost unchanged, and we concluded that their photo-

catalytic activities depend solely on morphology; the higher the OAP content is, the higher is the photocatalytic activity.

In this paper, we present results of detailed studies on structural/physical properties and photocatalytic activities of OAPs prepared under various conditions of US–HT processes. The aim of this study was to clarify the intrinsic reason for morphology-dependent photocatalytic activity of samples containing OAPs through photocatalytic-activity tests and analyses of structural/physical properties including time-resolved microwave conductivity (TRMC) measurements.

2 Experimental

2.1 Preparation of samples containing OAPs

OAP-containing samples were fabricated by US–HT processes using titanate nanowires (TNWs; Earthclean Tohoku Co. Ltd)[30] as a precursor, prepared by HT treatment of Evonik P25 titania (Nippon Aerosil) with a potassium hydroxide solution (17 mol L^{-1}) at 383 K for 20 h. In brief, the following procedure was used. TNWs (267 mg) were dispersed in 40 mL of Milli-Q water and ultrasonicated for 0–4 h at 298 K (US process). The suspension was then placed in a sealed Teflon bottle (100 mL) into which an additional 40 mL of Milli-Q water was added. Then the bottle was heated for 3–48 h at 413–473 K in an oven without agitation (HT process). Products were collected by centrifugation, washed with Milli-Q water, and dried under vacuum (353 K, 12 h).

2.2 Characterization

Specific surface areas of samples were estimated by nitrogen adsorption at 77 K using the Brunauer–Emmett–Teller (BET) equation. The morphology was studied by scanning electron microscopy (SEM; JEOL JSM-7400F), scanning transmission electron microscopy (STEM, HITACHI HD-2000) and transmission electron microscopy (TEM, JEOL JEM-2100F). Particles were classified by morphology into three groups based on the SEM analysis, as shown in Fig. 1, i.e., (a) OAP: an octahedral particle without observable defects, (b) semi-OAP: an octahedral particle with a defect (defects), and (c) others: an irregular shaped non-octahedral particle. The content of these particles in each sample was measured by counting at least 200 particles in several SEM images. However, there was no guarantee that the OAPs had no defects in their back side or in a part overlapped with another particle, and defects may have
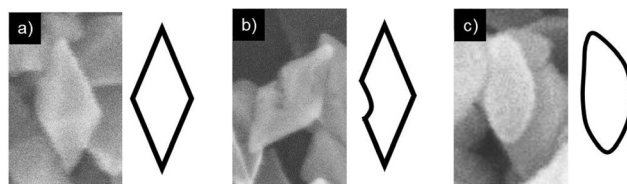

Fig. 1 Representative SEM images with respective models of (a) OAPs, (b) semi-OAPs and (c) others.

been too small to be detected. As reported in the ESI of our previous paper,[29] the ratio of OAPs to semi-OAPs was *ca.* 20–25%, and the sum of OAPs and semi-OAPs will hereafter be shown as "total OAP content".

Powder X-ray diffraction (XRD) analysis was performed using a Rigaku SmartLab diffractometer equipped with a sealed tube X-ray generator (a copper target; operated at 40 kV and 30 mA), a D/teX high-speed position-sensitive detector system and an ASC-10 automatic sample changer. All of the XRD analyses were performed under the following conditions: 2θ range, 10–90°; scan speed, 1.00° min⁻¹; and scan step, 0.008°. The obtained XRD patterns were analyzed by Rigaku PDXL, a crystal structure analysis package including Rietveld analysis,[31] installed in a computer controlling the diffractometer. Crystallite size was estimated from the corrected width of an anatase 101 diffraction peak using the Scherrer equation. Crystallinity of a sample was estimated using highly crystalline nickel oxide (NiO) as an internal standard. The standard (20.0 wt%) was mixed thoroughly with a sample (80.0 wt%) by braying in an agate mortar before XRD analysis. The crystallinity determination was based on the assumption that Rietveld analysis provides the weight fraction of each crystal among total crystalline components, and the weight fraction of an internal standard is overestimated if a sample mixture contains a non-crystalline component. Aspect ratio is defined as a ratio of average crystallite size (depth) vertical to {001} and {101} planes estimated by using a peak width of 004 and 101 diffraction peaks with the Scherrer equation.

The chemical formulas and atomic compositions of TNWs and HT products were determined by crystallinity, content of water, surface atomic content and bulk atomic content, which were examined by X-ray diffractometry (XRD), thermogravimetry (TG; ULVAC-RIKO TGD-9700), X-ray photoelectron spectroscopy (XPS; JEOL JPC-9010MC) and scanning electron microscopy with energy-dispersive X-ray spectroscopy (SEM/EDS, JEOL JSM-6360LA), respectively. The content of water was determined by TG based on the assumption that no volatile components other than water were included in the samples and thereby loss of weight was solely caused by removal of water. The SEM/EDS measurements were performed with an accelerating voltage higher than 15.0 kV and a working distance of 10 mm. Five different areas were analyzed for each sample and average data were used for determination of composition.

Photoabsorption properties of samples were measured by diffuse reflectance spectroscopy on a JASCO V-670 spectrophotometer equipped with a PIN-757 integrating sphere. Barium sulfate was used as the reference.

2.3 Photocatalytic activity test

Photocatalytic activities of samples were evaluated by measuring the rate of liberation of carbon dioxide (CO_2) or hydrogen (H_2) from a continuously stirred (1000 rpm) suspension of a sample (50 mg) in an aerated aqueous solution of acetic acid (5.0 mL, 5.0 vol%) (CO_2 system) or in a deaerated aqueous methanol solution (5.0 mL, 50 vol%) containing chloroplatinic

acid (corresponding to 2.0 wt% (as platinum) of a sample) for *in situ* platinum photodeposition (H_2 system), respectively. Photoirradiation (>290 nm) was performed with a 400 W high-pressure mercury lamp (Eiko-sha) at 298 K under magnetic stirring (1000 rpm). Amounts of liberated CO_2 and H_2 in a gas phase were measured by gas chromatography (TCD-GC). The photocatalytic activities were presented with reference to those of a commercial titania photocatalyst, FP-6 (Showa Denko Ceramic; anatase, specific surface area of *ca.* 100 m² g⁻¹ and crystalline size of 15 nm), of high-level photocatalytic activities similar to those of the well-known Evonik (Degussa) P25.[32]

2.4 Photoacoustic spectroscopy measurements

Double-beam photoacoustic spectroscopy (PAS) was used for estimation of total density of electron traps (ETs) in titania samples.[33] A dry sample powder was placed in a cell equipped with a quartz window. Two light beams were introduced into the cell through the window: a modulated visible-light beam to detect photoabsorption of trapped electrons by PAS and a continuous ultraviolet-light beam to excite titania and generate electron–hole pairs. The holes are consumed (removed) by oxidation of methanol introduced into the cell as a vapor, and electrons are captured by ETs. Upon irradiation with ultraviolet light, photoabsorption by trapped electrons increased to the saturated level, which corresponded to total density of ETs.

2.5 Time-resolved microwave conductivity measurements

Charge-carrier dynamics was studied by measuring time-resolved microwave conductivity (TRMC). The incident microwave of 36.8 GHz was generated by a Gunn diode of the K_a band, and UV laser pulses were created by the third harmonic of a 1064 nm Nd:YAG laser (10 Hz) with full width at half maximum of *ca.* 10 ns. Details of measurement and data processing have been reported elsewhere.[34,35]

3 Results and discussion

3.1 Characterization of a precursor

Structural/physical properties and photocatalytic activities of samples prepared in this study as well as precursor TNWs are summarized in Table 1. Fig. 2 shows the XRD pattern of TNWs, which resembles the pattern of potassium titanate, $K_2Ti_8O_{17}$ (International Centre for Diffraction Data, Powder Diffraction File 9874), but the peaks were less intense and broadened presumably due to the low crystallinity of TNWs, *i.e.*, presumably including amorphous titanates. No peaks attributed to anatase or rutile titania were observed. The composition of TNWs was determined to be $H_{1.32}K_{0.68}Ti_8O_{17}\cdot4.0H_2O$, corresponding to partially (*ca.* two-thirds) proton-exchanged potassium titanate (PEPT), by calculation based on the assumption that TNWs consisted of $H_{2-x}K_xTi_8O_{17}\cdot yH_2O$ without any titania (TiO_2) component using water content (11.1% corresponding to $18.02(y + (2 - x)/2)/\{1.01(2 - x) + 39.10x + 8 \times 47.87 + 17 \times 16.00 + 18.02y\}$) and

Table 1 Structural/physical properties and photocatalytic activities of samples prepared with various HT durations, HT temperatures and US durations

Code	US duration (h)	HT temperature (K)	HT duration (h)	Crystallinity (%)	Size (nm)	SSA[b] (m² g⁻¹)	Total OAP content (%)	d_{001}/d_{101}	Water (%)	K/Ti	K recovery[c] (%)	Composition[d] a	b	x	d_{ET}[e] (µmol g⁻¹)	TRMC[f] I_{max}	I_{40}/I_{max}[f]	I_{4000}/I_{max}[g]	Activity[g] CO₂ (%)	H₂ (%)
TNWs	0.0	—	0.0	0.0	—	360	—		11.1	0.085		0	4.0	0.7						
HD3	1.0	433	3.0	28.0	13	250	7	1.58	9.3	0.070	0.5	4	4.4	0.8	239	42	0.86	0.16	84	22
HD4.5	1.0	433	4.5	60.0	16	170	35	1.73	6.5	0.044	29	15	6.2	1.0	158	122	0.82	0.22	110	33
HD6[a]	1.0	433	6.0	78.0	17	124	64	1.71	4.5	0.025	105	37	8.6	1.1	114	139	0.86	0.20	145	37
HD9	1.0	433	9.0	83.0	19	85	62	1.66			135					124	0.84	0.18	102	30
HD12	1.0	433	12.0	83.0	19	81	61	1.65	3.2	0.011	74	49	7.5	0.6	98	103	0.92	0.22	87	26
HD24	1.0	433	24.0	81.0	19	80	62	1.64	2.4	0.011	209	40	4.2	0.5	65	108	0.85	0.19	88	28
HD48	1.0	433	48.0	82.0	20	78	60	1.63											85	32
HT413	1.0	413	6.0	38.0	14	255	7	1.57	8.5	0.059	0.3	6	4.8	0.8		32	0.77	0.14	75	22
HT423	1.0	423	6.0	54.0	15	209	39	1.71	7.9	0.060	30	12	6.7	1.2		66	0.83	0.15	98	30
HT433[a]	1.0	433	6.0	78.0	17	124	64	1.71	4.5	0.025	105	37	8.6	1.1	114	139	0.86	0.20	145	37
HT443	1.0	443	6.0	79.0	19	84	61	1.66											113	34
HT453	1.0	453	6.0	88.0	19	87	66	1.61	2.8	0.011	190	80	10.3	1.0		91	0.78	0.21	109	32
HT463	1.0	463	6.0	79.0	19	82	61	1.58											99	35
HT473	1.0	473	6.0	87.0	19	81	60	1.61	2.5	0.010	179	69	7.8	0.8		91	0.84	0.21	110	31
UD0	0.0	433	6.0	80.0	17	131	51	1.80	3.7	0.026		42	7.6	1.3	118	118	0.81	0.20	104	32
UD0.5	0.5	433	6.0	79.0	17	127	58	1.72	4.1	0.017		39	7.9	0.8	111	103	0.85	0.20	129	36
UD1[a]	1.0	433	6.0	78.0	17	124	64	1.71	4.5	0.025	105	37	8.6	1.1	114	139	0.86	0.20	145	37
UD1.5	1.5	433	6.0	75.0	17	129	56	1.66	3.7	0.021		29	5.4	0.8	108	116	0.85	0.22	127	36
UD2	2.0	433	6.0	80.0	17	130	53	1.77	3.9	0.030		43	8.2	1.5	108	113	0.84	0.19	121	35
UD3	3.0	433	6.0	76.0	17	122	50	1.70	4.1	0.022		32	6.6	0.9	113	100	0.89	0.24	121	33
UD4	4.0	433	6.0	78.0	17	129	45	1.73	4.1	0.021		36	7.5	0.9	111	88	0.84	0.20	101	27

[a] Samples HD6, HT433 and UD1 were all prepared with 1 h US duration, 433 K HT temperature and 6 h HT duration. [b] Specific surface area estimated by the BET equation. [c] Recovery of potassium calculated using the pH value of supernatant solutions after HT treatment and K/Ti ratio of products (see text). [d] Composition of products estimated using the formula $a\text{TiO}_2 \cdot \text{H}_{2-x}\text{K}_x\text{Ti}_8\text{O}_{17} \cdot b\text{H}_2\text{O}$. [e] Total density of electron traps (see text). [f] Results of time-resolved microwave conductivity measurements. I_{max}, I_{40} and I_{4000} are intensities (arbitrary) at maximum, at 40 nm and 4000 nm after a 355 nm laser pulse, respectively. [g] Relative photocatalytic activity with reference to that of Showa Denko Ceramics FP-6. CO₂ and H₂ correspond to systems of oxidative decomposition of acetic acid and methanol dehydrogenation with *in situ* deposited platinum (2 wt%), respectively.
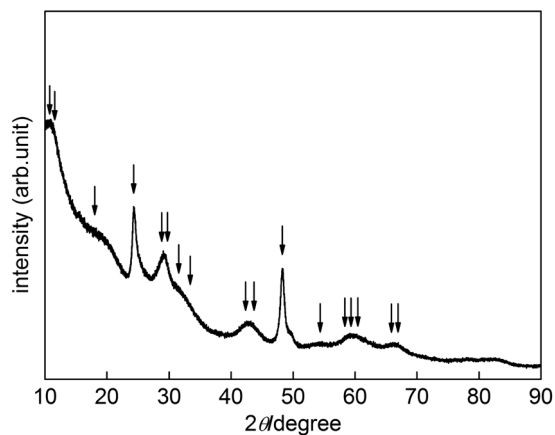
Fig. 2 An XRD pattern of TNWs. Arrows show the characteristic peaks of potassium titanate ($K_2Ti_8O_{17}$).

K/Ti ratio (0.085 corresponding to $x/8$) estimated by TG and EDS, respectively.

3.2 Composition of samples prepared under various US–HT reaction conditions

First, the influence of HT duration on the properties of products was examined using samples prepared with different HT durations (3–48 h), keeping the other synthesis parameters constant, *i.e.*, 433 K HT temperature, 1 h US duration and precursor concentration of 267 mg TNWs in 80 mL Milli-Q water. The XRD patterns of samples are shown in Fig. 3 (left panels). The wide range of patterns (left upper panel) indicates that the starting titanate is converted into anatase titania by HT treatment; a characteristic anatase peak at *ca.* 25.3° appeared with 3 h HT treatment and grew with prolonged HT duration (left upper and lower panels). An expanded view (left middle panel)
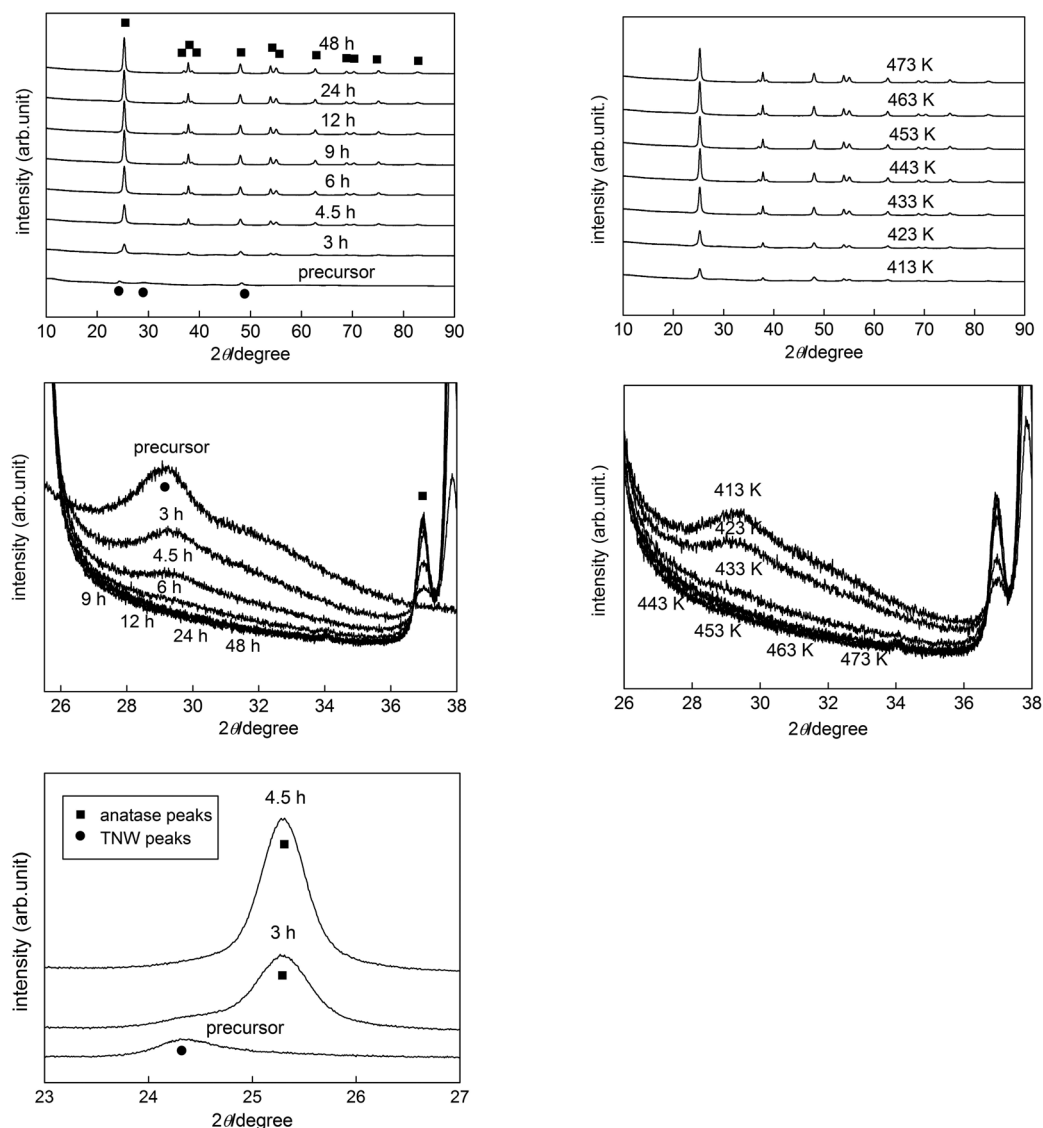

Fig. 3 XRD patterns of the precursor (TNWs) and products obtained with (left) various HT durations and (right) HT temperatures in various 2θ ranges.

at around 30° suggested that PEPT was still included in the samples even after 6 h HT treatment. Intensity of anatase peaks seemed to be almost saturated by 9 h HT treatment with disappearance of peaks attributed to titanate, suggesting complete crystallization with this HT duration. However, as shown in Table 1, Rietveld analysis of XRD patterns of samples mixed with an internal standard (nickel oxide) indicated that crystalline content of anatase, the sole crystalline component, reached a constant level of *ca.* 83% with 9–12 h HT treatment, and the 12 h-HT sample still contained an appreciable amount of potassium (*ca.* 12% of potassium in the precursor). The composition of products was estimated using the formula $a\text{TiO}_2 \cdot \text{H}_{2-x}\text{K}_x\text{Ti}_8\text{O}_{17} \cdot b\text{H}_2\text{O}$ based on the assumption that only anatase (a part of "$a\text{TiO}_2$") is crystalline giving XRD peaks; coefficients a, b and x were calculated using the data of crystallinity ($79.87 \times a$/[total molar mass]), K/Ti ratio ($x/(a+8)$) and water content ($18.02 \times \{b + (2-x)/2\}$/[total molar mass]) as shown in Table 1. The potassium content in the amorphous part of samples, x, did not greatly change during HT treatment, but it increased slightly by prolonging HT duration (and by higher HT temperature as discussed later) and then decreased. This suggests that the precursor TNWs were homogeneous PEPT without phase separation and were converted into anatase titania with dissolution of the potassium component as potassium hydroxide, *i.e.*,

$$\text{H}_{1.32}\text{K}_{0.68}\text{Ti}_8\text{O}_{17} \cdot 4.0\text{H}_2\text{O} \rightarrow 8\text{TiO}_2 + 4.32\text{H}_2\text{O} + 0.68\text{KOH}. \quad (1)$$

In fact, the pH of the reaction mixture after HT treatment increased, being consistent with the stoichiometry. Assuming that the pH change was solely responsible for potassium-hydroxide release and that the titanium component was not dissolved in the reaction mixture by HT treatment, molar amounts of potassium ion (i) in a supernatant solution and (ii) expected to be released from TNWs could be calculated by using the pH value of supernatant solutions and K/Ti ratio of products. The recovery of potassium ion, (i)/(ii) (Table 1) seemed reasonable to support the potassium release, though some of them exceed 100% possibly due to a relatively large error in (i) especially higher pH and the fact that titanium component might be dissolved by HT.

The above-described results do not exclude the possibility of the presence of amorphous titania, *i.e.*, the titanate part ($\text{H}_{2-x}\text{K}_x\text{Ti}_8\text{O}_{17}$) is a mixture of amorphous titania and potassium titanate (($8 - 4x)\text{TiO}_2 \cdot 0.5x\text{K}_2\text{Ti}_8\text{O}_{17} \cdot (1 - 0.5x)\text{H}_2\text{O}$). However, our recent study has shown that post-calcination of samples prepared in the same way even at 1173 K does not change the crystallinity or cause phase transition from anatase to rutile.[36] This suggests the absence of amorphous titania in the samples prepared with longer HT durations. Thus, it is concluded that HT treatment converted TNWs into a mixture of anatase crystallites and amorphous PEPT.

The presence of PEPT in the final product is not surprising since the HT process proceeds to reach an equilibrium in the reaction mixture, *i.e.*, between PEPT and anatase with a sodium hydroxide solution (eqn (1)): TNWs were prepared through the backward reaction of eqn (1) using an anatase–

rutile mixture with a much higher concentration of potassium hydroxide. Similar equilibria have already been reported for the synthesis of anatase nanowires,[37] nanotubes,[38,39] microspheres[40] and rutile nanorod films.[41] A study on the preparation through a HT process using diluted acid instead of water or a two-step HT process in water to shift the equilibrium to the titania side is now in progress to obtain purer OAP samples.

The structural/physical properties of the products, *i.e.*, crystallite size, crystallinity and specific surface area, prepared with different durations are summarized in Fig. 4 (upper
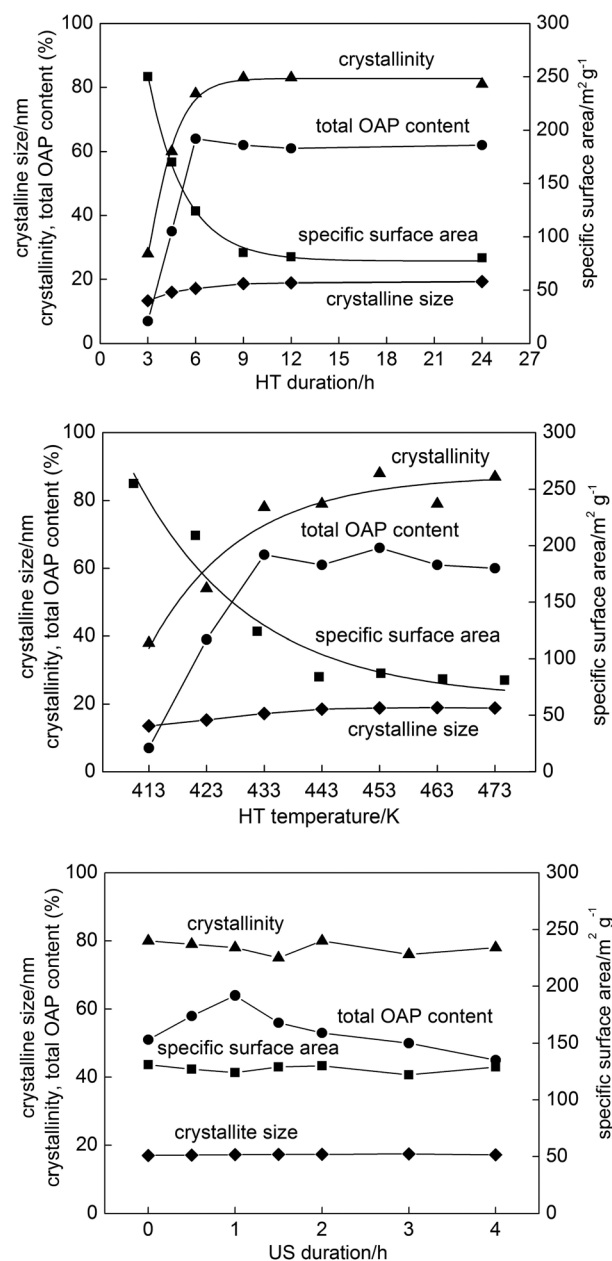

Fig. 4 Crystallinity, crystalline size, specific surface area and total OAP content as functions of (upper) HT duration, (middle) HT temperature and (lower) US duration.

panel). As expected, prolonged HT duration caused larger crystallite size, lower specific surface area and higher crystallinity reaching plateaus after 9 h HT duration of *ca.* 19 nm, 80 m^2 g^{-1} and 83%, respectively. Thus, under the conditions of 433 K HT temperature and 1 h US duration, 9 h HT duration was sufficient to convert TNWs into crystallized anatase titania.

It has been reported that properties of HT products strongly depended on HT temperature for various HT processes, *e.g.*, synthesis of square bismuth tungstate (Bi$_2$WO$_6$) nanoplates,[42] reduction of graphene oxide to graphene,[43] preparation of nanosize rutile and anatase,[23] synthesis of manganese(IV) oxide nanowires/nanorods,[44] and phase transition of amorphous titania to anatase.[45] Therefore, the influence of HT temperature on properties of samples was investigated for samples prepared at different HT temperatures (413–473 K) with no change in the other synthesis parameters, *i.e.*, 6 h HT duration, 1 h US duration and precursor concentration of 267 mg TNWs in 80 mL Milli-Q water. Table 1 and Fig. 3 (right panels) also show the influence of HT temperature on products prepared with 1 h US and 6 h HT durations; change in XRD patterns in Fig. 3 seemed similar to that with different HT durations, and the samples prepared even at higher HT temperatures still contained amorphous PEPT. The composition of products changed with elevation of HT temperature, the trend of which was similar to that with prolonged HT duration; the higher the HT temperature was, the higher, lower and larger were the crystallinity, specific surface area and crystallite size, which reached plateaus of *ca.* 80%, 80 m^2 g^{-1} and 19 nm, respectively, at a HT temperature of 433 K (Fig. 4, middle panel). This finding is consistent with the above-mentioned reaction mechanism considering that the equilibrium between PEPT and anatase titania is almost constant regardless of the HT temperature, and HT temperature of 433 K may be sufficient to reach the equilibrium.

On the other hand, US duration is expected to have no influence on composition of the product under the given conditions of HT temperature and duration since the US process for breaking TNWs is unlikely to affect the equilibrium in the HT reaction (eqn (1)). In fact, as shown in Fig. 4 (lower panel), the influence of US duration (before HT treatment at 433 K for 6 h) on the composition of products seemed negligible, *i.e.*, crystallinity, specific surface area and crystallite size were almost constant at *ca.* 80%, 125 m^2 g^{-1} and 17 nm, respectively, as was reported previously[29] (as there was a negligible difference in XRD patterns as shown in Fig. S1 in the ESI†). The significant exception is morphology, which depended on US duration, as discussed in the next section.

3.3 Particle morphology of samples prepared under various US–HT conditions

Fig. 5 shows representative SEM and TEM images of the product prepared by 1 h US and 6 h HT treatment at 433 K, which was one of the samples with the highest crystallinity (78%) and total OAP content (64%). As clearly seen in the SEM images, many of the particles had an octahedral morphology (see also Fig. S2–4 in the ESI†). The inset TEM image (Fig. 5,
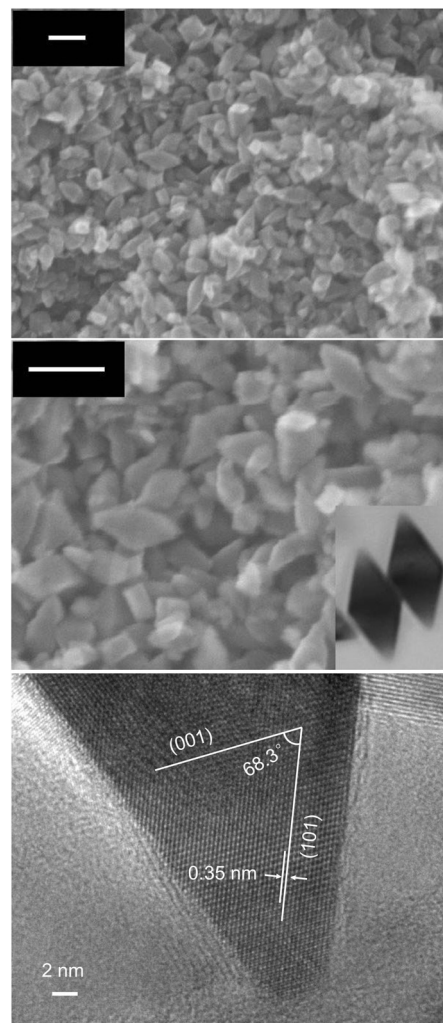

Fig. 5 (upper/middle) Typical SEM images of a product prepared by 6 h HT (433 K and 1 h US). Scale bars correspond to 50 nm. (inset) A TEM image of OAPs. (lower) The corresponding high-resolution TEM image.

middle panel) shows diamond-shaped particles with lower contrast tops, consistent with the decreasing thickness in the direction vertical to the electron beam in TEM near the apical ends of an OAP. A high-resolution image (Fig. 5, lower panel) showed fringes corresponding to (101) and (001) lattice spacings and the angle (68.3°) between them, as has already been reported previously.[16]

As shown in Fig. 4, total OAP content was increased and almost saturated when HT duration was prolonged (upper) or HT temperature was raised (middle), indicating that the HT process led to the production of OAPs from TNWs. A slight decrease in total OAP content after saturation at 6 h and at 433 K might be due to transformation of OAPs under more severe conditions as has been reported for HT synthesis of hematite; dissolution of the spindle-like precursor started from the apexes with new {001} facet formation.[46] The total OAP content was, roughly speaking, almost proportional to crystallinity for all of the samples prepared with the same US
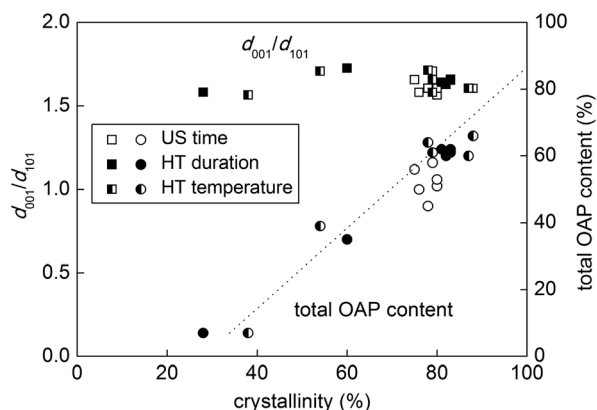
Fig. 6 Correlations of total OAP content (circles) and aspect ratio (squares) with crystallinity.

duration (1 h) as shown in Fig. 4. Fig. 6 shows plots of total OAP content and aspect ratio d_{001}/d_{101} as a function of crystallinity. Higher HT temperature and longer HT duration (closed and half-closed circles, respectively) caused higher crystallinity and, at the same time, higher total OAP content, suggesting a constant ratio of total OAP to total anatase particles independent of HT duration and temperature when the same US duration was used. Extrapolation of a possible linear line to 100% crystallinity suggests a maximum total OAP content of ca. 85%, not 100%, presumably due to the existence of the potassium component, which cannot be converted into anatase. On the other hand, samples prepared with different US durations (6 h HT duration, 433 K HT temperature, and 267 mg TNWs suspended in 80 mL Milli-Q water) showed differences in total OAP content, though the crystallinity was almost constant (see Fig. 4, lower panel), i.e., particle morphology was highly dependent on the initial structural properties, mainly the morphology, of the precursor TNWs. Ultrasonication (US) has generally been used as a pre-treatment process to obtain a homogeneous suspension for reaction to make products uniform.[47,48] In the present study, however, another function of US was suggested, i.e., US changed morphology of substrates by breaking TNWs. The morphological change caused by the US process is shown in Fig. S5 (ESI†); nanowire bundles seemed to be broken by US, but the extent of breakage could not be evaluated quantitatively.

Aspect ratio (d_{001}/d_{101}; AR) was introduced as an alternative parameter to evaluate particle morphology. Since XRD patterns give averaged data on crystallites, AR may be a better parameter representing how particles spire; the higher the AR value is, the higher is the extent of OAPs. In a previous report on thermal treatment of OAP-containing particles,[37] AR, which changed between ca. 0.9 and 1.7, was used to discuss morphology. For the samples used in the present study, low-crystallinity (<0.4) samples exhibited AR lower than 1.6, though AR values for the others were in a narrow range of 1.6–1.7, and it seemed difficult to discuss the difference between them. Actually, as can be seen in Fig. 6, plots of AR were scattered,

presumably due to the possible relatively large error in estimation of d_{001} from a small 004 peak. On the basis of these considerations, total OAP content seems better than AR for evaluation of particle morphology in this study, but further discussion is still needed. In the following sections, total OAP content will be mainly used for discussion of morphology-dependent photocatalytic activities.

3.4 Electron-trap density and TRMC response of samples prepared under various US–HT conditions

One of the most important properties characterizing heterogeneous photocatalysts is the amount of crystalline defects on which either recombination of charge carriers (electrons and holes) or adsorption of reactants can occur, resulting in photocatalytic activity reduction or enhancement, respectively.[49–51] In general, products obtained at a higher temperature exhibit higher crystallinity and thus have fewer lattice defects.[33,52] The amounts of lattice defects in products obtained at different HT and US durations were studied by the DB-PAS method as density of electron traps (ET density), i.e., density of vacant electron-trapping sites was measured. It is presumed that such ETs may capture photoexcited electrons and induce recombination with holes, if the depth from the bottom of the conduction band (CB) is large so as not to allow thermal reexcitation to the CB. The results are shown in Fig. 7 as a function of specific surface area for samples prepared with different HT durations. The longer the HT duration was, the lower was the specific surface area, and ET density was decreased in proportion to specific surface area. This suggests that ETs are located mainly on the surface or near the surface, and their density is constant, ca. 0.6 nm^{-2}, which is comparable to that of commercial titania samples.[46] This is consistent with the fact that ET density of samples prepared under the conditions of different US durations with the HT duration (6 h) and temperature (433 K) kept constant was almost the same as shown in
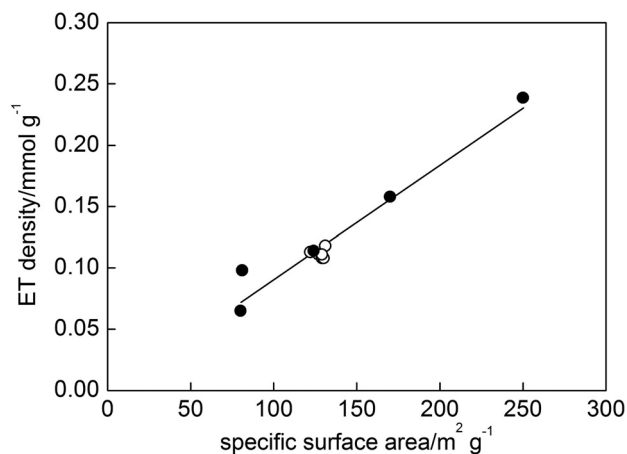

Fig. 7 Electron trap (ET) density as a function of specific surface area. Closed and open circles show data for samples prepared with different HT and US durations, respectively.

Fig. 4 (lower panel) since specific surface areas of those samples were negligibly changed with change in US duration.

Thus, the samples prepared with different US durations had almost constant structural/physical properties, including crystallinity, crystallite size, specific surface area and ET density, except for particle morphology (total OAP content), which may predominantly govern their photocatalytic activity as will be discussed later.

As a measure of mobility and lifetime of charge carriers, time-resolved microwave conductivity (TRMC) was investigated for the samples as shown in Fig. 8. The TRMC signal (arbitrary) was increased with a 355 nm laser pulse (*ca.* 10 ns) which excites titania to produce photoexcited electrons and holes and then decayed after the laser pulse in a ns to μs time scale. The signal intensity is considered to be proportional to the summation of products of mobility and number (density) of each charge carrier, *i.e.*, to overall mobility of charge carriers, and therefore, *e.g.*, even when the number of charges is small, the intensity is enhanced if their mobility is high and *vice versa*. It has been suggested that holes, which are charge carriers, generated in irradiated titania particles are quickly trapped in certain sites to contribute negligibly to the TRMC signal. On the basis of these assumptions, the signal in Fig. 8 is attributable to the number and mobility of photoexcited electrons. In the analysis, two parameters were extracted. One is the maximum intensity of TRMC signal (I_{max}) corresponding to overall mobility of photoexcited electrons in relaxed states after laser excitation. Since it was suggested in a previous report on femtosecond-laser spectroscopic measurement that photoexcited electrons in photocatalysts are readily trapped by
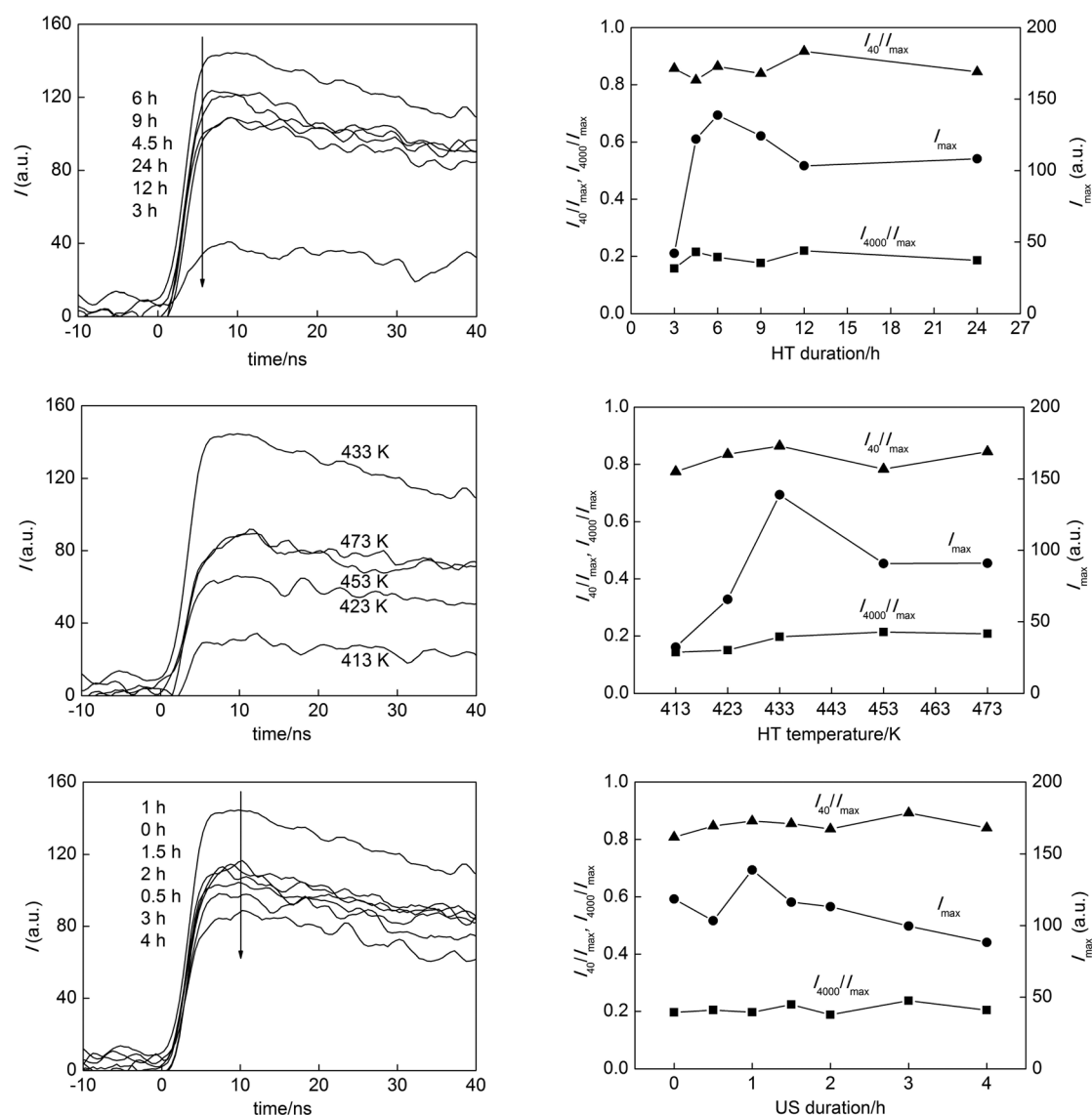

Fig. 8 (left) Time-course of TRMC signal and (right) parameters of samples prepared with different (upper) HT durations, (middle) HT temperatures and (lower) US durations.

shallow ETs below the conduction band within a few ps,[53] I_{max} might reflect the migration of electrons being trapped in shallow traps and detrapped thermally to the conduction band, *i.e.*, density of such shallow traps. The other parameter is the rate of signal decay. There should be at least two reasons for the signal decay: decrease in the number (density) of electrons due to recombination with trapped holes and decrease in mobility due to trapping in deeper ETs, leading to low mobility of electrons. Since the TRMC decay profiles could not be fitted with a single exponential function in general, the extent of decay was evaluated by decrease after 40 and 4000 ns as I_{40}/I_{max} and I_{4000}/I_{max}, respectively.

It is clear from Fig. 8 (right panels) that signal decay is independent of the preparation conditions; I_{40}/I_{max} and I_{4000}/I_{max} were *ca.* 0.8 and 0.2, respectively, for all of the samples in this study, indicating that the density of deep ETs reducing signal intensity in the present samples was not greatly different. Our recent study on post-treatment of OAPs showed appreciable effects of calcination and grinding on TRMC signal decay,[36] suggesting that the change in particle shape from OAPs to sintered aggregates and round-edged particles resulted in a change in the distribution of the ETs in the particles. Consequently, the negligible difference in decay profiles in the present samples is attributable to OAP-shaped morphology without sintering and/or thermal blunting.

On the other hand, I_{max} changed significantly depending on the preparation conditions, HT duration, HT temperature and US duration, and the patterns of change in I_{max} shown in Fig. 8 (right panels) resembled those of total OAP content shown in Fig. 4. Fig. 9 shows the relation of I_{max}, as well as ET density, with total OAP content. Though the plots were rather scattered (presumably due to the fact that I_{max} also depends on other structural/physical properties), I_{max} seems to increase with increase in total OAP content (ET density decreased with increase in total OAP content). It should be noted that I_{max} was almost proportional to total OAP content when limited to a series of samples prepared with different US durations that

exhibited almost constant structural/physical properties including ET density (Fig. 9). This finding indicates that particle morphology governs charge-carrier (photoexcited electrons) dynamics. A hypothesis is that {101} facets selectively exposed on OAPs possess ETs suitable for trapping with higher mobility on their surface structure. The results of a theoretical study on this hypothesis will be reported in the near future. In any case, a significant point is that US duration-controlled samples are structurally or physically different from each other only in total OAP content and charge carrier dynamics.

3.5 Correlation between properties and photocatalytic activity

The correlation between properties and photocatalytic activities was studied using photocatalytic reactions of oxidative decomposition of acetic acid (CO_2 system) and dehydrogenation of methanol (H_2 system) as shown in Fig. 10. In both reaction systems, certain conditions, 6 h HT duration, 433 K HT temperature and 1 h US duration, gave maximum photocatalytic activities. The maximum activity in the CO_2 system was *ca.* 1.5 times (150%) of that of commercial Showa Denko Ceramics FP-6, one of the most active photocatalysts, while the maximum activity in the H_2 system was *ca.* 40% of that of FP-6. The reason for the low levels of photocatalytic activity in the H_2 system is still unknown. It has been suggested that {001} facets with higher surface energy are necessary for efficient separation of charge carriers,[54] and alcohol molecules could be preferentially adsorbed on {001} facets, leading to efficient charge separation. It was also reported that platinum particles were photodeposited preferentially on {101} facets of decahedral anatase particles (DAPs) exposing eight {101} and two {001} facets and showed a high level of photocatalytic activity but DAPs with platinum photodeposited on both facets showed much lower photocatalytic activity than that of DAP with platinum only on {101} facets.[55] Thus, platinum deposition as a requisite for hydrogen evolution might be a key issue for activity in the H_2 system, and further studies on OAP activity in the H_2 system are presently being conducted.

For samples prepared under the conditions with different HT durations and HT temperatures, it must be scientifically unacceptable to find a correlation between only one structural property and photocatalytic activity since all properties changed simultaneously with HT duration and HT temperature. In the conventional understanding, a balance between high crystallinity and sufficient specific surface area might be responsible for the highest photocatalytic activity of the sample prepared with 6 h HT at 433 K; in both cases, curves of plots of crystallinity and specific surface area crossed at this condition, 6 h and 433 K, though this coincidence should be occasional. It was reported that sufficient specific surface area resulting in a large amount of adsorbed substrates enhances the rate of capture of electrons and holes in them, while high crystallinity results in a lower density of lattice defects to reduce the rate of recombination of electrons and holes, and thus photocatalytic activity is enhanced.[56,57] The differences in photoabsorption properties could be also considered as the
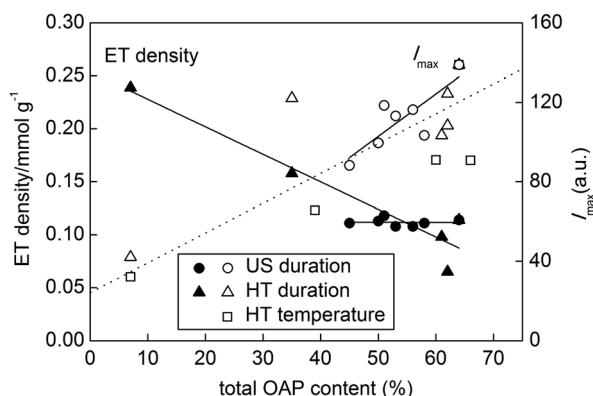
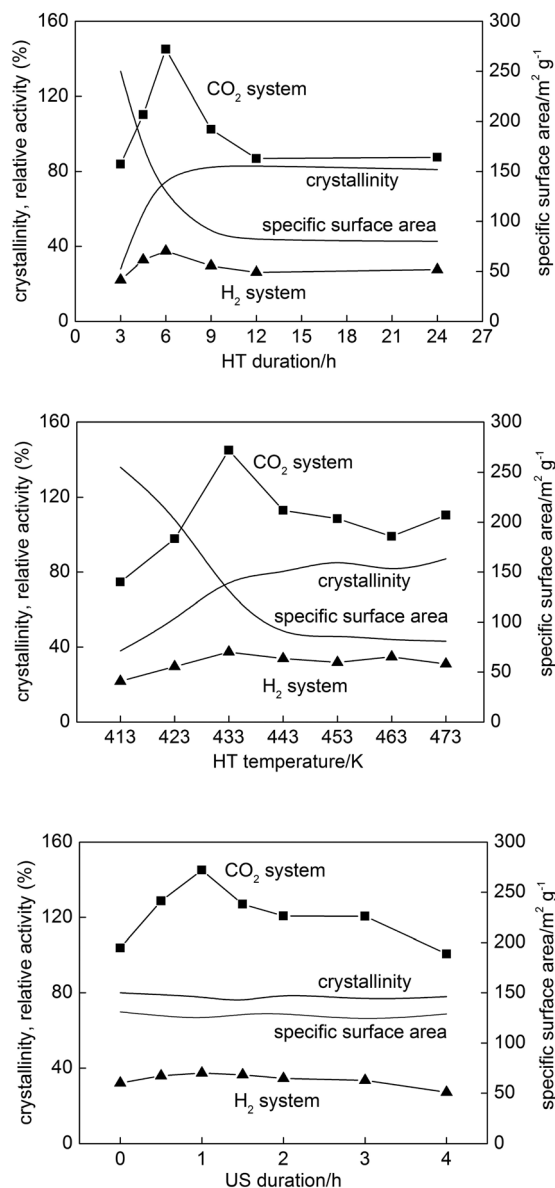**Fig. 9** ET density (closed) and I_{max} (open) as functions of total OAP content.

Fig. 10 Photocatalytic activities of samples prepared with different (upper) HT durations, (middle) HT temperatures and (lower) US durations. Changes in crystallinity and specific surface area as representative conventional structural properties are also plotted.

as photoabsorption properties and morphology influenced the resulting photocatalytic activity. Thus, the most important aspect was to prepare samples differing in only morphology, which we succeeded in by application of various US durations.

It should be noted that the maximum activity of the sample among those prepared with different US durations cannot be interpreted, at least for these samples, by the balance of specific surface area and crystallinity or photoabsorption properties, since those structural properties were almost the same (Fig. 10 and S6, bottom). In other words, the activity could be explained by the particle morphology, which was the sole structural parameter that varied depending on the US duration as discussed in the preceding section. Thus, our previous communication[29] showed for the first time, as far as we know, morphology-dependent photocatalytic activity excluding the possible dependence on other structural/physical properties of photocatalyst particles such as crystallinity, composition, specific surface area and crystalline size. Fig. 11 (upper) shows the dependence of photocatalytic activities on total OAP content. A general trend of the activity being increased with increasing total OAP content was seen in both systems, but the plots were rather scattered except for the data for samples prepared with different US durations. Assuming that photo-
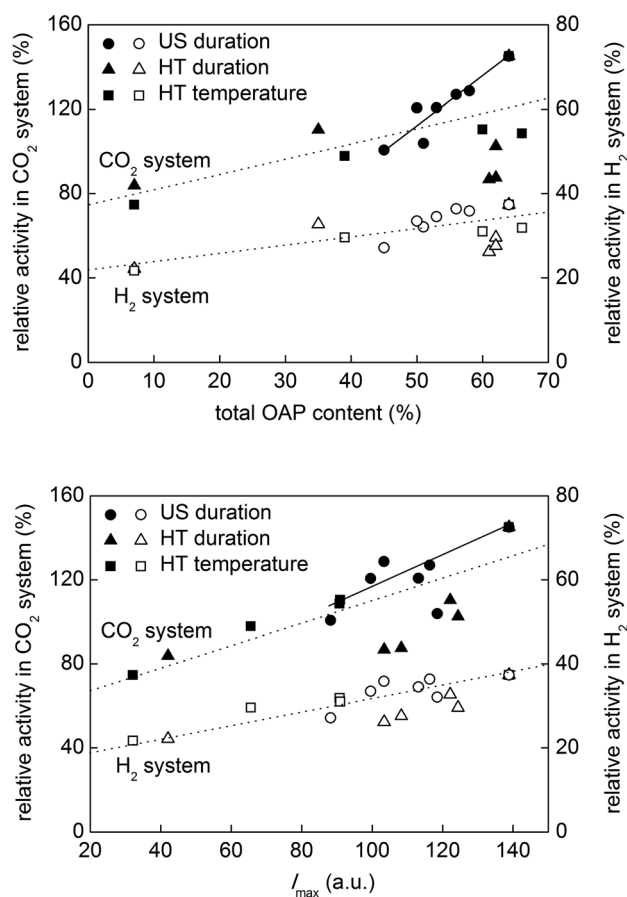

Fig. 11 Photocatalytic activities of samples as functions of (upper) total OAP content and (lower) I_{max}.

reason for higher photocatalytic activity since with increase of HT duration particle size increased and more photons could be absorbed, as shown by diffuse reflectance spectra (DRS) in the left part of Fig. S6.† However, samples prepared at 4.5, 6 and 12 h possessed almost the same photoabsorption properties, but highly differed in photocatalytic activity, and increase of HT duration to 24 h resulted in a further increase in the photoabsorption range, but no change in crystalline size and photocatalytic activity was noticed. For samples prepared at various HT durations and HT temperatures all parameters changed simultaneously and thus various properties, i.e., balance between crystallinity and specific surface area, as well

catalytic activities of OAPs and semi-OAPs are equal, the linear part of dependence on US duration-controlled samples in the CO_2 system suggests that photocatalytic activities of pure OAPs should be *ca.* 230% of the photocatalytic activity of FP-6. Preparation of HT products with higher OAP content by modification of the present US–HT procedure is presently underway.

Then, how does particle morphology control the photocatalytic activity? A hint can be seen in Fig. 9 showing the correlation between I_{max} and total OAP content. The possible dependence of photocatalytic activities on I_{max} is shown in Fig. 11 (lower). Since, again, the samples prepared with different US durations have similar structural/physical properties except for total OAP content, the difference in the charge-carrier dynamics must be morphology-dependent. Therefore, a possible reason for the morphology-dependent photocatalytic activity may be related to ETs on the facets controlling the charge-carrier dynamics. As has been described in the preceding section, a hypothesis is that {101} facets selectively exposed on OAPs possess ETs suitable for trapping electrons loosely and thus keeping their mobility high on their surface structure, and the shallow traps might work as sites for one-electron reduction of molecular oxygen adsorbed on the surface but not for transfer of electrons to platinum deposited on the surface.

4 Conclusions

In summary, conditions of the ultrasonication–hydrothermal (US–HT) process significantly influenced structural/physical properties of OAP-containing products. Changes in HT duration or HT temperature resulted in simultaneous changes in all structural/physical properties, *i.e.*, crystallinity, crystallite size, specific surface area, ET density and morphology. Therefore, a direct correlation between only one property and photocatalytic activity could not be shown. However, change in US duration resulted in the generation of HT products being different in morphology with all of the other structural properties being almost constant. Thus, the authors were able to conclude that morphology, represented empirically by total OAP content, governs the photocatalytic activity of OAP-containing samples, and the higher the OAP content is, the higher is the photocatalytic activity. The intrinsic reason for the morphology-dependent activity is still ambiguous at present, but the fact that TRMC-intensity maximum was almost proportional to total OAP content suggests that shallow ETs on the surface of exposed {101} facets are preferable especially for one-electron reduction of oxygen adsorbed on the surface to drive oxidative decomposition of organic compounds. On the basis of the above discussion, further studies are needed to clarify the intrinsic mechanism of titania photocatalysis. There is a need to prepare purer OAPs, to confirm their superior photocatalytic activity, by modification of the present US–HT process, which has been started in our laboratory, and analysis of the energy-resolved distribution of ETs on OAP-containing

samples is also needed. A methodology to realize this has been developed, and preliminary results have been obtained and will be reported in the near future.

Acknowledgements

References

1 U. Diebold, *Surf. Sci. Rep.*, 2003, **48**, 53–229.
2 A. Fujishima, X. Zhang and D. Tryk, *Surf. Sci. Rep.*, 2008, **63**, 515–582.
3 X. Chen and S. S. Mao, *Chem. Rev.*, 2007, **107**, 2891–2959.
4 A. Kudo and Y. Miseki, *Chem. Soc. Rev.*, 2009, **38**, 253–278.
5 H. M. Zhang, Y. H. Han, X. L. Liu, P. R. Liu, H. Yu, S. Q. Zhang, X. D. Yao and H. J. Zhao, *Chem. Commun.*, 2010, **46**, 8395–8397.
6 B. Ohtani, *Chem. Lett.*, 2008, **37**, 217–229.
7 B. Ohtani, *Phys. Chem. Chem. Phys.*, 2014, **16**, 1788–1797.
8 O.-O. Prieto-Mahaney, N. Murakami, R. Abe and B. Ohtani, *Chem. Lett.*, 2009, **38**, 238–239.
9 G. Liu, C. Sun, H. G. Yang, S. C. Smith, L. Wang, G. Q. Lu and H. M. Cheng, *Chem. Commun.*, 2010, **46**, 755–757.
10 S. W. Liu, J. G. Yu and W. G. Wang, *Phys. Chem. Chem. Phys.*, 2010, **12**, 12308–12315.
11 A. G. Agrios and P. Pichat, *J. Photochem. Photobiol., A*, 2006, **180**, 130–135.
12 E. Kowalska, O. O. Prieto-Mahaney, R. Abe and B. Ohtani, *Phys. Chem. Chem. Phys.*, 2010, **12**, 2344–2355.
13 D. Friedmann, C. Mendive and D. Bahnemann, *Appl. Catal., B*, 2010, **99**, 398–406.
14 J. Z. Chen, H. Bin Yang, J. W. Miao, H. Y. Wang and B. Liu, *J. Am. Chem. Soc.*, 2014, **136**, 15310–15318.
15 M. Li, W. Hebenstreit, U. Diebold, A. M. Tyryshkin, M. K. Bowman, G. G. Dunham and M. A. Henderson, *J. Phys. Chem. B*, 2000, **104**, 4944–4950.
16 F. Amano, T. Yasumoto, O. O. Prieto-Mahaney, S. Uchida, T. Shibayama and B. Ohtani, *Chem. Commun.*, 2009, 2311–2313.
17 F. Amano, T. Yasumoto, O. O. P. Mahaney, S. Uchida, T. Shibayama, Y. Terada and B. Ohtani, *Top. Catal.*, 2010, **53**, 455–461.
18 D. V. Bavykin, J. M. Friedrich and F. C. Walsh, *Adv. Mater.*, 2006, **18**, 2807–2824.
19 Z. Wei, Y. Liu, H. Wang, Z. Mei, J. Ye, X. Wen, L. Gu and Y. Xie, *J. Nanosci. Nanotechnol.*, 2012, **12**, 316–323.
20 X. G. Han, Q. Kuang, M. S. Jin, Z. X. Xie and L. S. Zheng, *J. Am. Chem. Soc.*, 2009, **131**, 3152–3153.

21 P. D. Cozzoli, A. Kornowski and H. Weller, *J. Am. Chem. Soc.*, 2003, **125**, 14539–14548.

22 C. C. Wang and J. Y. Ying, *Chem. Mater.*, 1999, **11**, 3113–3120.

23 H. M. Cheng, J. M. Ma, Z. G. Zhao and L. M. Qi, *Chem. Mater.*, 1995, **7**, 663–671.

24 M. Hirano and M. Takahashi, *J. Mater. Sci.*, 2014, **49**, 8163–8170.

25 R. L. Penn and J. F. Banfield, *Geochim. Cosmochim. Acta*, 1999, **63**, 1549–1557.

26 D. C. Manfroi, A. dos Anjos, A. A. Cavalheiro, L. A. Perazolli, J. A. Varela and M. A. Zaghete, *Ceram. Int.*, 2014, **40**, 14483–14491.

27 N. Murakami, Y. Kurihara, T. Tsubota and T. Ohno, *J. Phys. Chem. C*, 2009, **113**, 3062–3069.

28 H. X. Li, Z. F. Bian, J. Zhu, D. Q. Zhang, G. S. Li, Y. N. Huo, H. Li and Y. F. Lu, *J. Am. Chem. Soc.*, 2007, **129**, 8406–8407.

29 Z. Wei, E. Kowalska and B. Ohtani, *Chem. Lett.*, 2014, **43**, 346–348.

30 S. Uchida and Y. Sanehira, *Jpn. Pat.*, P2005-162584A, 2005.

31 B. Ohtani, R. M. Bowman, D. P. Colombo, H. Kominami, H. Noguchi and K. Uosaki, *Chem. Lett.*, 1998, 579–580.

32 B. Ohtani, O. O. Prieto-Mahaney, D. Li and R. Abe, *J. Photochem. Photobiol., A*, 2010, **216**, 179–182.

33 N. Murakami, O. O. P. Mahaney, R. Abe, T. Torimoto and B. Ohtani, *J. Phys. Chem. C*, 2007, **111**, 11927–11935.

34 E. Kowalska, H. Remita, C. Colbeau-Justin, J. Hupka and J. Belloni, *J. Phys. Chem. C*, 2008, **112**, 1124–1131.

35 Z. Hai, N. El Kolli, D. Uribe, P. Beaunier, M. Jose-Yacaman, J. Vigneron, A. Etcheberry, S. Sorgues, C. Colbeau-Justin, J. Chena and H. Remita, *J. Mater. Chem. A*, 2013, **1**, 10829–10835.

36 Z. Wei, E. Kowalska and B. Ohtani, *Molecules*, 2014, **19**, 19573–19587.

37 H. B. Wu, H. H. Hng and X. W. Lou, *Adv. Mater.*, 2012, **24**, 2567–2571.

38 H. Yin, H. Liu and W. Z. Shen, *Nanotechnology*, 2010, **21**, DOI: 10.1088/0957-4484/21/3/035601.

39 J. L. Tao, J. L. Zhao, C. C. Tang, Y. R. Kang and Y. X. Li, *New J. Chem.*, 2008, **32**, 2164–2168.

40 X. Y. Hu, T. Zhang, Z. Jin, S. Z. Huang, M. Fang, Y. C. Wu and L. Zhang, *Cryst. Growth Des.*, 2009, **9**, 2324–2328.

41 J. M. Wu and B. Qi, *J. Am. Ceram. Soc.*, 2007, **90**, 657–660.

42 C. Zhang and Y. F. Zhu, *Chem. Mater.*, 2005, **17**, 3537–3545.

43 Y. Zhou, Q. L. Bao, L. A. L. Tang, Y. L. Zhong and K. P. Loh, *Chem. Mater.*, 2009, **21**, 2950–2956.

44 X. Wang and Y. D. Li, *Chem. – Eur. J.*, 2003, **9**, 300–306.

45 K. Yanagisawa and J. Ovenstone, *J. Phys. Chem. B*, 1999, **103**, 7781–7787.

46 C. J. Jia, L. D. Sun, Z. G. Yan, L. P. You, F. Luo, X. D. Han, Y. C. Pang, Z. Zhang and C. H. Yan, *Angew. Chem., Int. Ed.*, 2005, **44**, 4328–4333.

47 N. Sakai, R. Wang, A. Fujishima, T. Watanabe and K. Hashimoto, *Langmuir*, 1998, **14**, 5918–5920.

48 Z. Zhong, F. Chen, A. S. Subramanian, J. Lin, J. Highfield and A. Gedanken, *J. Mater. Chem.*, 2006, **16**, 489–495.

49 N. Murakami, O. O. P. Mahaney, T. Torimoto and B. Ohtani, *Chem. Phys. Lett.*, 2006, **426**, 204–208.

50 B. Ohtani, *J. Photochem. Photobiol., C*, 2010, **11**, 157–178.

51 B. Ohtani, O. O. P. Mahaney, F. Amano, N. Murakami and R. Abe, *J. Adv. Oxid. Technol.*, 2010, **13**, 247–261.

52 N. Murakami, R. Abe and B. Ohtani, *Chem. Phys. Lett.*, 2008, **451**, 316–320.

53 D. E. Skinner, D. P. Colombo, J. J. Cavaleri and R. M. Bowman, *J. Phys. Chem.*, 1995, **99**, 7853–7856.

54 T. Ohno, K. Sarukawa and M. Matsumura, *New J. Chem.*, 2002, **26**, 1167–1170.

55 C. Liu, X. Han, S. Xie, Q. Kuang, X. Wang, M. Jin, X. Xie and L. Zheng, *Chem. – Asian J.*, 2013, **8**, 282–289.

56 H. Kominami, T. Matsuura, K. Iwai, B. Ohtani, S. Nishimoto and Y. Kera, *Chem. Lett.*, 1995, 693–694.

57 J. G. Yu, Q. J. Xiang, J. R. Ran and S. Mann, *CrystEngComm*, 2010, **12**, 872–879.